Orientational Disorder Drives Site Disorder in Plastic Ammonia Hemihydrate

Niccolò Avallone,[1] Simon Huppert,[1] Philippe Depondt,[1] Leon Andriambariarijaona,[2] Frédéric Datchi,[2] Sandra Ninet,[2] Thomas Plé,[3] Riccardo Spezia,[3] and Fabio Finocchi[1]

[1]*Sorbonne Université, CNRS UMR 7588, Institut des NanoSciences de Paris, INSP, 75005 Paris, France*

[2]*Sorbonne Université, Muséum National d'Histoire Naturelle, CNRS UMR 7590, Institut de Minéralogie, de Physique des Matériaux et de Cosmochimie, IMPMC, 75005 Paris, France*

[3]*Laboratoire de Chimie Théorique (LCT), CNRS and Sorbonne Université, Paris, France*

(Received 20 November 2023; accepted 24 July 2024; published 4 September 2024)

In the 2–10 GPa pressure range, ammonia hemihydrate $H_2O:(NH_3)_2$ (AHH) is a molecular solid in which intermolecular interactions are ruled by distinct types of hydrogen bonds. Upon heating, the low-temperature ordered $P2_1/c$ crystal (AHH-II) transits to a bcc phase (AHH-*p*bcc) where each site is randomly occupied by water or ammonia. In addition to the site disorder, experiments suggest that AHH-*p*bcc is a plastic solid, but the physical origin and mechanisms at play for the rotational and site disordering remain unknown. Using large-scale ($\sim 10^5$ atoms) and long-time (> 10 ns) simulations, we show that, as temperature rises above the transition line, orientational disorder sets in, breaking the strongest hydrogen bonds that provide the largest contribution to the cohesion of the ordered AHH-II phase and enabling the molecules to migrate from a crystal site to a neighboring one. This generates a plastic molecular alloy with site disorder while the solid state is overall maintained until melting at a higher temperature. The case of high (P, T) plastic ammonia hemihydrate can be extended to other water-ammonia alloys where a similar interplay between distinct hydrogen bonds occurs.

DOI: 10.1103/PhysRevLett.133.106102

The existence of exotic magnetic fields in icy planets [1] could be linked to the presence of water, ammonia, and methane mixtures [2–4] in their cores, whose phase diagrams are only partially known. At ambient pressure and low temperatures, water-ammonia mixtures crystallize into three stable compositions with 2:1, 1:1, and 1:2 H_2O/NH_3 ratios, namely the ammonia di, mono, and hemihydrates (ADH, AMH, and AHH, respectively) [5]. As water is more abundant than ammonia in the solar system [6–8], the water-poorest AHH solid was believed unlikely to exist in the mantle of planets, and it has thus attracted less attention. However, several experiments showed that ADH and AMH dehydrate under pressure into mixtures of AHH and ice [9–11], thus indicating that AHH could be present at extreme conditions. As ice is denser than AHH, the dehydration could have important consequences regarding the composition of the interior of icy planets and convective processes [11,12].

The renewed interest for the ammonia hemihydrate led to the recent discovery of several new phases under high pressure. Among them stands the AHH-*p*bcc phase reported in Refs. [13,14], which was obtained either by heating the monoclinic AHH-II crystal in the range 3.5–10 GPa, or by compression of the liquid above 320 K, as illustrated in the phase diagram in Fig. 1. Experiments showed that AHH-*p*bcc is a body-centered cubic (bcc) crystal in which water and ammonia molecules are randomly arranged on the lattice sites [14]. This site disorder is characteristic of an alloy and contrasts with the fully ordered molecular configuration of the AHH-II crystal [11]. Other disordered molecular alloys were previously observed in AMH [15,16] and ADH [10], for which exotic properties such as partial ionization [17] and plasticity [18] were reported. By similarity with AMH, Andriambariarijaona *et al.* [14] suggested that AHH-*p*bcc is a plastic crystal characterized by dynamical orientational disorder, but this has not been directly confirmed by direct measurements to date. Other important and unsettled questions are the physical origin of the site disorder, and the microscopic mechanisms at play in the transition from the fully site-ordered phase at low T to the site-disordered phase at high T.

This Letter aims at obtaining a comprehensive understanding of the onset of the rotational and site disorder in the AHH-*p*bcc phase through simulations that are closely compared with the recently available experimental data [14]. We employed a molecular dynamics approach, simulating a large number ($\geq 10^5$) of atoms over long times (≥ 10 ns), which enables the description of dynamical effects on ns timescales and an accurate statistical sampling. We reproduce the main experimental findings and provide a complete description at the atomic level of the static and dynamical properties of AHH-*p*bcc. In particular, we show that the transition from the fully ordered low-T crystal to the site-disordered plastic alloy is driven by fast molecular rotations that disrupt the H-bond network on a

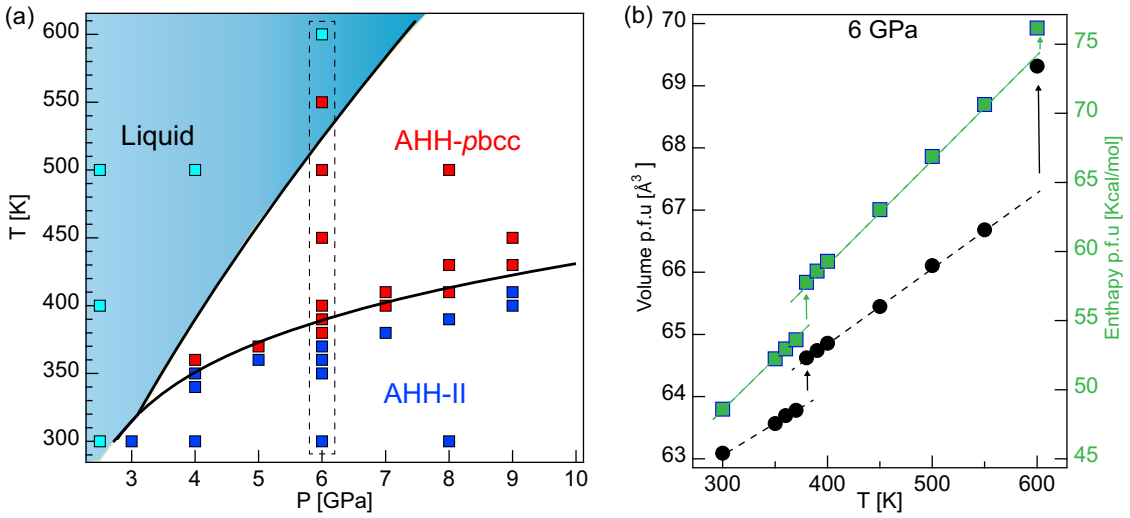

FIG. 1. (a) Experimental phase diagram of AHH (P < 10 GPa) adapted from Ref. [14]. Blue, red, and turquoise squares refer to simulated AHH-II, AHH-*p*bcc, and liquid phases, respectively. The dashed box highlights the simulation data along the 6 GPa isobar. (b) Evolution of mean volume V (black circles) and enthalpy H (teal squares) per formula unit versus temperature along the 6 GPa isobar as obtained by the simulations. The arrows highlight the discontinuities in V (black) and H (green).

few ps timescale and enable site exchanges between the molecules.

We performed constant temperature, constant pressure molecular dynamics simulations using the Tinker-HP package [19,20]. The force field parametrization used for the ammonia molecules is OPLS-AA [21,22], whereas for water molecules we used the SPC/Fw flexible model potential [23,24]. We employed a classical Langevin thermostat and an anisotropic Langevin barostat, for a system consisting of 36×10^3 molecules. The simulation time lengths span from a few to several tens of nanoseconds, depending on the required equilibration time at each temperature. Further details are given in Supplemental Material (SM) [25], Sec. I and Sec. II.

The (P, T) simulations points (colored symbols), revealing three distinct phases, are presented in Fig. 1(a), and compare very well with the recently updated experimental phase diagram of AHH (lines) from Ref. [14] in the range 2–10 GPa, 300–650 K. For the following description of the phase transitions, we focus on the results obtained at 6 GPa fixed pressure. The evolution with temperature of the volume and enthalpy of the simulated system, from 300 to 600 K along the 6 GPa isobar, presented in Fig. 1(b), shows two concomitant discontinuities, which are the signatures of two phase transitions. The first one occurs at $T_c = 375 \pm 5$ K, thus very close to the AHH-II to AHH-*p*bcc experimental transition temperature of 390 K [13,14]. Furthermore, the x-ray structure factor of the simulated system above T_c (SM, Fig. S5), matches very well the experimental one for AHH-*p*bcc. These facts conspire to identify the simulated transition as that from AHH-II to AHH-*p*bcc. In addition, the simulated AHH-II and AHH-*p*bcc coexistence line, which lies between the blue (AHH-II) and red (AHH-*p*bcc) points, is fully consistent with the experiments.

By direct inspection of the atomic structure and of several observables (see further on), we identify the second transition ($T_m = 575 \pm 25$ K @ 6 GPa) to the melting of the AHH-*p*bcc solid. It occurs close to the experimental value ($T_m = 525$ K). All of the above observations show that our simulations faithfully reproduce the available experimental results. We note, however, that, upon cooling, the system does not recover the enthalpy and lattice parameters of AHH-II (SM, Fig. S2). This suggests that the backward transition is kinetically hindered within the size ($\sim 10^5$ atoms) and timescale ($\lesssim 50$ ns) of our simulations.

To determine whether AHH-*p*bcc qualifies as a plastic solid with orientational disorder [37], we analyze the molecular rotations of the dipoles associated with each NH_3 and H_2O molecule in the solid below and above T_c, as well as the breaking and reforming of intermolecular hydrogen bonds. Figure 2 shows some representative snapshots of the 6 GPa simulations at 300, 500, and 600 K, viewed along the **a** axis of the AHH-II crystal. For the sake of clarity, only a thin slab of the simulation box comprising three adjacent (100) planes is represented. Interestingly, at 300 K [Fig. 2(a)], water molecules display the same orientation in all (100) layers, at variance with the ammonia molecules. A closer look to the system dynamics reveals that, already at this temperature, NH_3 molecules rotate around their molecular axes. This is also the direction of the OH···N hydrogen bonds, which, among the four possible H bonds, are the strongest (the four kinds of hydrogen bonds, ranked from the strongest to the weakest are [38] OH···N, OH···O, NH···O, and NH···N). In

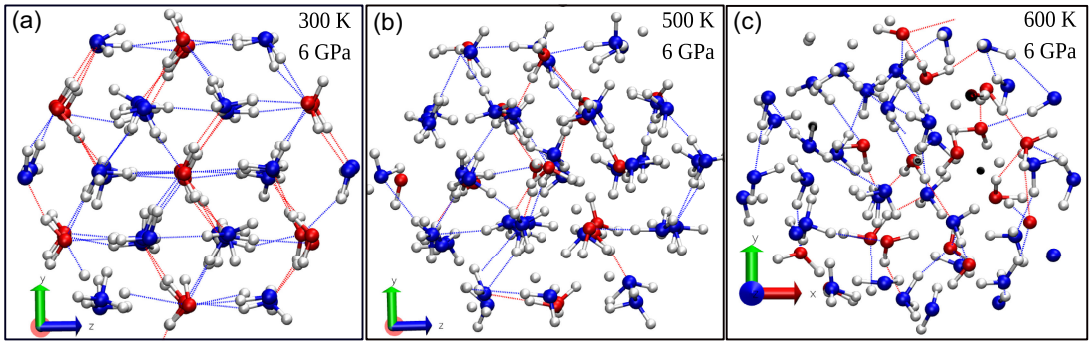

FIG. 2. Snapshots of the simulated AHH alloys at three different temperatures (300, 500, and 600 K) and 6 GPa. The portions of the structures are seen along the **a** crystal axis of the simulation box, that is, on few (100) planes.

the AHH-II crystal, these bonds are stable over long timescales (∼0.1 ns) and contribute the most to the crystal cohesion (see also SM, Fig. S7). In contrast, in the 500 K snapshot [Fig. 2(b)], the AHH-II alternation between ammonia and water sites is lost; water and ammonia molecules within distinct (100) planes have different orientations. H bonds are considerably weakened in this phase, being constantly broken and reformed, in a similar way as in the liquid [Fig. 2(c)). This is consistent with the experimental observation that the OH···N stretch Raman band present in AHH-II disappears in the high-temperature phase [14].

This regime is characteristic of a plastic solid with orientational disorder and is confirmed on more quantitative grounds by Fig. 3, which shows the time-dependent dipole autocorrelation functions $\langle \mathbf{u}_i(0)\mathbf{u}_i(t)\rangle$, with $\mathbf{u_i}$ the unit vector along the water or ammonia molecular dipole ($i = H_2O$ or NH_3, respectively), for each simulated T at 6 GPa (see SM, Sec. IV for more details). The results change drastically at T_c. Below T_c, $\langle \mathbf{u}_i(0)\mathbf{u}_i(t)\rangle$ displays a small drop in the first ps, which is due to the fast librational motion, followed by a slowly decreasing tail, showing that molecular orientations persist on ∼100 ps timescales at least. Above T_c, in contrast, both H_2O and NH_3 dipoles loose memory of their orientation in less than 10 ps (see Table SII in SM for the characteristic decay times). Thus, orientational disorder has fully settled in, which is the signature of the plastic solid.

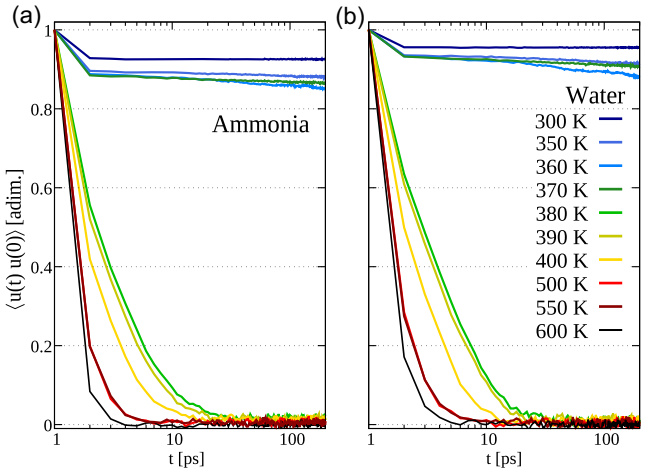

FIG. 3. Dipole time-dependent correlation functions $\langle \mathbf{u}_i(0)\mathbf{u}_i(t)\rangle$ of NH_3 (a) and H_2O molecules (b), for temperatures between 300 and 600 K at $P = 6$ GPa.

Uncorrelated molecular rotations imply the breaking (and making) of hydrogen bonds. The H-bond lifetimes are collected in Table I (see also SM, Fig. S7). The two trends for the time-dependent dipole autocorrelation functions and the H-bond lifetimes τ_j ($j = $ OH···N, OH···O, NH···O, NH···N) are intertwined: both vary drastically between the AHH-II crystal and the AHH-*p*bcc plastic solid. Below T_c, the strongest OH···N bonds display the longest lifetimes ($50 \leq \tau_{OH\ldots N} \leq 160$ ps), while $\tau_{NH\ldots X} \simeq$ 5–20 ps (X = O, N). OH···O bonds only appear above T_c in the plastic phase, in which all H-bond lifetimes are only a few ps and continue decreasing with temperature down to about 1 ps at 500 K.

The simulations thus reveal that in the AHH-*p*bcc phase, NH_3 and H_2O molecules rotate almost freely, breaking and forming hydrogen bonds with lifetimes on the ps timescale. However, at variance with the liquid phase ($T \geq 600$ K), the molecular centers of mass sit on the sites of the bcc lattice. Such a behavior is characteristic of a plastic solid [37].

TABLE I. Hydrogen bond lifetimes.

$T(K)$	$\tau_{OH\cdots O}$ (ps)	$\tau_{NH\cdots N}$ (ps)	$\tau_{NH\cdots O}$ (ps)	$\tau_{OH\cdots N}$ (ps)
300	···	12	18	160
350	···	7.4	11	66
360	···	6.6	7.5	49
370	···	6.0	7.2	44
380	2.6	1.7	1.8	2.8
390	2.3	1.6	1.6	2.5
400	1.7	1.3	1.4	1.9
500	1.2	0.8	1.0	0.9
600	0.8	0.6	0.7	0.7

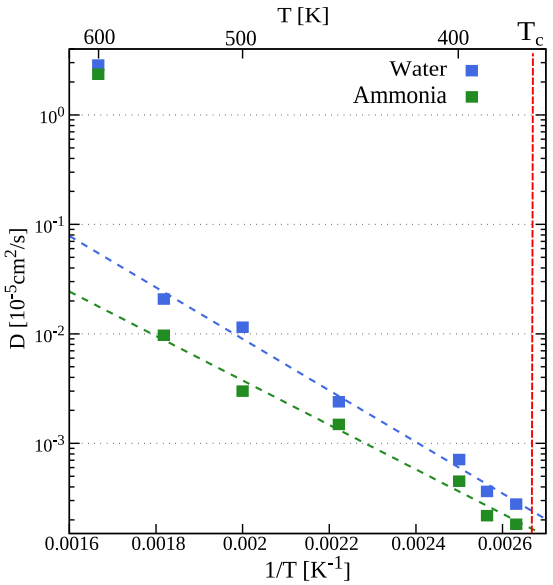

FIG. 4. Diffusion coefficients D, as computed from the mean square displacements of the center of mass of water and ammonia molecules in the plastic and liquid phases. The Arrhenius fits of $D(T)$ for the water and ammonia molecules in the plastic phase are drawn with dashed lines.

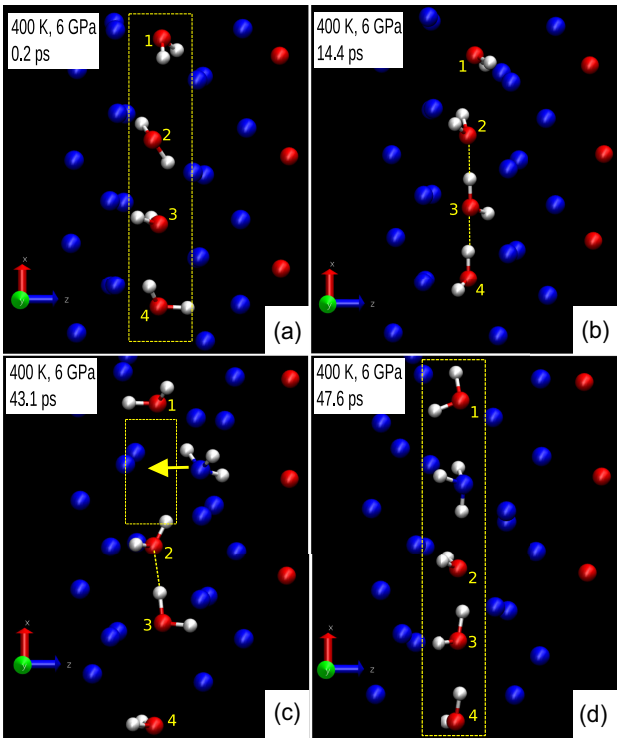

FIG. 5. Snapshots of simulation at 400 K and 6 GPa (see text). Blue, red, and white balls are nitrogen, oxygen, and hydrogen atoms, respectively. For clarity sake, we did not draw hydrogen atoms that are not directly involved in hydrogen bonds with the diffusing molecules.

We are now left with the explanation for the formation of the disordered molecular alloy (DMA) in the AHH-$p$bcc phase. In the following, we clarify how the bcc crystal sites can be occupied randomly by a water or an ammonia molecule, starting from a well ordered phase [see the comparison between Figs. 2(a) and 2(b)]. To this purpose, we compute the evolution with temperature of the diffusion coefficients of H_2O and NH_3 at P = 6 GPa, reported in Fig. 4. Below T_c, the molecular mean displacements are smaller than a few hundredths of Å. There is no diffusion among sites in the AHH-II crystal at the nanosecond timescale, which is confirmed by the absence of site exchanges between ammonia and water molecules when inspecting the initial and final configurations. In sharp contrast, above T_c the diffusion coefficient becomes measurable and rapidly increases with temperature by 2 orders of magnitude between T_c and the melting temperature, following an Arrhenius-like trend. In the plastic solid, both NH_3 and H_2O molecules can translate on average by ∼0.1 Å at 380 K and ∼1 Å at 500 K in 1 ns.

Because of the molecular diffusion, when the AHH-II crystal is heated above T_c, the chemical order is permanently modified into a DMA, and the cubic AHH-$p$bcc phase is found. In particular, the onset of orientational disorder enables the restructuring of the initial molecular configuration of AHH-II and, consequently, of the H-bond network. Our simulations thus highlight that the site disorder characteristic of the DMA phase is driven by the dynamical rotational disorder. We call this process orientational-disorder-driven site disorder.

To obtain further insight into how site substitutions occur, we show a representative event occurring during the simulation at 6 GPa and 400 K. Figure 5 shows snapshots of the simulation at different times, focusing on a region where site exchanges can be visually detected. Panel A displays the initial configuration (the AHH-II crystal) shortly after (0.2 ps) the beginning of the simulation. The column highlighted by a yellow rectangle contains only water molecules. Later on (panel B), molecular rotations have taken place, altering the hydrogen bond network. The crystal cohesion is thus altered and a gap opens between the water molecules labeled 1 and 2 (panel C). Then, an ammonia molecule moves into this gap and the highlighted area now contains a NH_3 molecule (panel D). This example of a site exchange, which originates from the dynamical reorientations of the OH···N bonds, illustrates how the restructuring of the AHH-II crystal network can lead to the DMA AHH-$p$bcc phase on the nm (length) and ns (time) scales above T_c. Although plastic solids are often characterized by the free rotation of molecules, self-diffusion coefficients have also been measured via radio tracer techniques [37,39]. Here, we point out that molecular self-diffusion and the eventual formation of a disordered molecular alloy in ammonia hemihydrate are triggered by orientational disorder: the two phenomena are thus correlated.

In conclusion, our results are fully consistent with the available experimental data [14]. Long simulation times (≥ 10 ns) and large simulation boxes ($\simeq$10 nm linear sizes) are necessary to obtain atomic-scale insight into the very nature of the transition mechanism leading to the AHH-*p*bcc plastic phase. Solid AHH is ruled by strongly angle-dependent hydrogen bonds, which provide the main contribution to the cohesion of the AHH-II crystal; as water and ammonia molecules have distinct symmetries, this induces a geometrical frustration resulting in the monoclinic lattice. At the transition, the orientational-disorder-driven site disorder promotes molecular diffusion propagating defect-mediated exchange processes that eventually lead to a full substitutional disorder between water and ammonia on the crystal sites. As orientational and site disorder sets in, the solid adopts a more symmetric cubic phase.

The combination of a molecular alloy with directional hydrogen bonds is likely a key to this new type of solids with orientational and site disorder. Interestingly, other ammonia-water alloys at high pressure [14,17] show disordered plastic phases, which might be driven by orientational disorder as well. Plastic behavior has also been observed in pure ammonia Ice [40] and theoretically proposed in water Ice VII [41]. The generalization of the orientational-disorder-driven molecular diffusion process to other hydrogen-bonded solids is an open issue.

Acknowledgments—This work was granted access to the HPC resources of TGCC under the allocation A0130906719 made by GENCI. N. A. received support from a Ph.D. fellowship with the Institut des Sciences du Calcul et des Données (ISCD) of Sorbonne Université. S. N., L. A. and F. D. acknowledge financial support from the french Agence Nationale de la Recherche under Grant No. ANR-15-CE30-0008-01 (SUPER-ICES).

[1] S. Stanley and J. Bloxham, Nature (London) **428**, 151 (2004).
[2] J. I. Lunine and D. J. Stevenson, Icarus **70**, 61 (1987).
[3] F. Hersant, D. Gautier, and J. Lunine, Planet. Space Sci. **52**, 623 (2004).
[4] Y. Alibert and O. Mousis, Astron. Astrophys. **465**, 1051 (2007).
[5] A. D. Fortes and M. Choukroun, Space Sci. Rev. **153**, 185 (2010).
[6] W. B. Hubbard, Science **214**, 145 (1981).
[7] C. Cavazzoni, G. L. Chiarotti, S. Scandolo, E. Tosatti, M. Bernasconi, and M. Parrinello, Science **283**, 44 (1999).
[8] T. Guillot, Annu. Rev. Earth Planet Sci. **33**, 493 (2005).
[9] A. D. Fortes, I. G. Wood, M. Alfredsson, L. Vočadlo, K. S. Knight, W. G. Marshall, M. G. Tucker, and F. Fernandez-Alonso, High Press. Res. **27**, 201 (2007).
[10] J. S. Loveday, R. J. Nelmes, C. L. Bull, H. E. Maynard-Casely, and M. Guthrie, High Press. Res. **29**, 396 (2009).
[11] C. W. Wilson, C. L. Bull, G. Stinton, and J. S. Loveday, J. Chem. Phys. **136**, 094506 (2012).
[12] X. Li, W. Shi, X. Liu, and Z. Mao, Am. Mineral. **104**, 1307 (2019).
[13] C. W. Wilson, C. L. Bull, G. W. Stinton, D. M. Amos, M.-E. Donnelly, and J. S. Loveday, J. Chem. Phys. **142**, 094707 (2015).
[14] L. Andriambariarijaona, F. Datchi, H. Zhang, K. Béneut, B. Baptiste, N. Guignot, and S. Ninet, Phys. Rev. B **108**, 174102 (2023).
[15] J. S. Loveday and R. J. Nelmes, Phys. Rev. Lett. **83**, 4329 (1999).
[16] H. Zhang, F. Datchi, L. M. Andriambariarijaona, G. Zhang, J. A. Queyroux, K. Béneut, M. Mezouar, and S. Ninet, J. Chem. Phys. **153**, 154503 (2020).
[17] C. Liu, A. Mafety, J. A. Queyroux, C. W. Wilson, H. Zhang, K. Béneut, G. L. Marchand, B. Baptiste, P. Dumas, G. Garbarino, F. Finocchi, J. S. Loveday, F. Pietrucci, A. M. Saitta, F. Datchi, and S. Ninet, Nat. Commun. **8**, 1065 (2017).
[18] H. Zhang, F. Datchi, L. Andriambariarijaona, M. Rescigno, L. E. Bove, S. Klotz, and S. Ninet, J. Phys. Chem. Lett. **14**, 2301 (2023).
[19] L. Lagardère, L.-H. Jolly, F. Lipparini, F. Aviat, B. Stamm, Z. F. Jing, M. Harger, H. Torabifard, G. A. Cisneros, M. J. Schnieders, N. Gresh, Y. Maday, P. Y. Ren, J. W. Ponder, and J.-P. Piquemal, Chem. Sci. **9**, 956 (2018).
[20] O. Adjoua, L. Lagardère, L. H. Jolly, A. Durocher, T. Very, I. Dupays, Z. Wang, T. J. Inizan, F. Cèlerse, P. Ren, J. W. Ponder, and J. P. Piquemal, J. Chem. Theory Comput. **17**, 2034 (2021).
[21] W. L. Jorgensen and J. Tirado-Rives, J. Am. Chem. Soc. **110**, 1657 (1988).
[22] W. L. Jorgensen, D. S. Maxwell, and J. Tirado-Rives, J. Am. Chem. Soc. **118**, 11225 (1996).
[23] Y. Wu, H. L. Tepper, and G. A. Voth, J. Chem. Phys. **124**, 024503 (2006).
[24] F. Paesani, W. Zhang, D. A. Case, T. E. Cheatham, and G. A. Voth, J. Chem. Phys. **125**, 184507 (2006).
[25] See Supplemental Material, which includes Refs. [26–36], at http://link.aps.org/supplemental/10.1103/PhysRevLett.133.106102 for additional computational details, for a more developed analysis of the phase transition mechanism and its identification from the simulation data, for the comparison of the simulated and experimental x-ray diffraction patterns as well as additional data on the rotational dynamics and on the hydrogen bond network.
[26] U. Essmann, L. Perera, M. L. Berkowitz, T. Darden, H. Lee, and L. G. Pedersen, J. Chem. Phys. **103**, 8577 (1995).
[27] X.-Z. Li, B. Walker, and A. Michaelides, Proc. Natl. Acad. Sci. U.S.A. **108**, 6369 (2011).
[28] S. Huppert, T. Plé, S. Bonella, P. Depondt, and F. Finocchi, Appl. Sci. **12**, 4756 (2022).
[29] S. Schaack, E. Mangaud, E. Fallacara, S. Huppert, P. Depondt, and F. Finocchi, Phys. Rev. Lett. **131**, 126101 (2023).
[30] B. Leimkuhler and C. Matthews, J. Chem. Phys. **138**, 174102 (2013).
[31] B. Leimkuhler and C. Matthews, Proc. R. Soc. A **472**, 0138 (2016).
[32] M. Tuckerman, B. J. Berne, and G. J. Martyna, J. Chem. Phys. **97**, 1990 (1992).

[33] S. E. Feller, Y. Zhang, R. W. Pastor, and B. R. Brooks, J. Chem. Phys. **103**, 4613 (1995).
[34] A. P. Thompson, H. M. Aktulga, R. Berger, D. S. Bolintineanu, W. M. Brown, P. S. Crozier, P. J. in 't Veld, A. Kohlmeyer, S. G. Moore, T. D. Nguyen, R. Shan, M. J. Stevens, J. Tranchida, C. Trott, and S. J. Plimpton, Comput. Phys. Commun. **271**, 108171 (2022).
[35] S. Coleman, D. Spearot, and L. Capolungo, Model. Simul. Mater. Sci. Eng. **21**, 055020 (2013).
[36] A. Luzar and D. Chandler, Nature (London) **379**, 55 (1996).
[37] J. N. Sherwood, *The Plastically Crystalline State* (John Wiley & Sons, New York, 1979).
[38] J. Řezáč and P. Hobza, J. Chem. Theory Comput. **9**, 2151 (2013).
[39] A. V. Chadwick, J. M. Chezeau, R. Folland, J. W. Forrest, and J. H. Strange, J. Chem. Soc. Faraday Trans. **71**, 1610 (1975).
[40] S. Ninet, F. Datchi, and A. M. Saitta, Phys. Rev. Lett. **108**, 165702 (2012).
[41] A. Toffano, J. Russo, M. Rescigno, U. Ranieri, L. E. Bove, and F. Martelli, J. Chem. Phys. **157**, 094502 (2022).